Geophysical Research Letters

RESEARCH LETTER
10.1029/2021GL092912

Key Points:

- Jupiter's cloud-level wind profile extended to depth, matches in sign and amplitude both the measured odd and residual-even gravity harmonics
- The majority of the signal comes from the wind profile between 25°S and 25°N, which must extend unaltered thousands of kilometers deep
- The gravity signal also implies that from the cloud-tops downward the flow must be organized in a columnar structure and also decay radially

Supporting Information:

Supporting Information may be found in the online version of this article.

Correspondence to:

E. Galanti,
eli.galanti@weizmann.ac.il

Citation:

Galanti, E., Kaspi, Y., Duer, K., Fletcher, L., Ingersoll, A. P., Li, C., et al. (2021). Constraints on the latitudinal profile of Jupiter's deep jets. *Geophysical Research Letters*, *48*, e2021GL092912. https://doi.org/10.1029/2021GL092912

Received 13 FEB 2021
Accepted 9 APR 2021

Constraints on the Latitudinal Profile of Jupiter's Deep Jets

Eli Galanti[1], Yohai Kaspi[1], Keren Duer[1], Leigh Fletcher[2], Andrew P. Ingersoll[3], Cheng Li[4], Glenn S. Orton[5], Tristan Guillot[6], Steven M. Levin[5], and Scott J. Bolton[7]

[1]Department of Earth and Planetary Sciences, Weizmann Institute of Science, Rehovot, Israel, [2]School of Physics and Astronomy, University of Leicester, Leicester, UK, [3]California Institute of Technology, Pasadena, CA, USA, [4]Department of Climate and Space Sciences and Engineering, University of Michigan, Ann Arbor, MI, USA, [5]Jet Propulsion Laboratory, California Institute of Technology, Pasadena, CA, USA, [6]Observatoire de la Cote d'Azur, Nice, France, [7]Southwest Research Institute, San Antonio, TX, USA

Abstract The observed zonal winds at Jupiter's cloud tops have been shown to be closely linked to the asymmetric part of the planet's measured gravity field. Here, we examine to what extent, and at which latitudes, must the flows at depth resemble those at the cloud level to match the gravity signal. We show, using both the symmetric and asymmetric parts of the measured gravity field, that the observed cloud-level wind profile between 25°S and 25°N must extend unaltered to depths of thousands of kilometers. Poleward, the midlatitude deep jets also contribute to the gravity signal, but might differ somewhat from the cloud-level winds. We analyze the likelihood of this difference and give bounds to its strength. We also find that to match the gravity measurements, the winds must project inward in the direction parallel to Jupiter's spin axis, and decay inward in the radial direction.

Plain Language Summary Observations of Jupiter's cloud-tops reveal very strong atmospheric winds reaching 500 km/hr. Using very accurate measurements of the planet's gravity field, provided by NASA's Juno spacecraft, the cloud-level winds were found to extend thousands of kilometers into the interior of Jupiter, with a wind profile similar to that observed at the clouds level. However, analysis of various measurements suggested that at some latitudinal regions the flow below the clouds might be different to some extent. Here we explore the constraints posed by the Juno gravity measurements on the latitudinal profile of the zonal flow in Jupiter below the cloud level. We find that to explain the detailed latitudinal structure of the wind-attributed gravity field, the cloud-level winds in the 60°S–60°N range have to extend deep into the planet, approximately keeping their observed latitudinal profile. With that, we find that most of the wind-induced gravity signal comes from the 25°S to 25°N region, where the strongest jets reside, suggesting that in the midlatitudes the observed jets at the cloud level might be somewhat different at depth.

1. Introduction

The zonal (east-west) winds at Jupiter's cloud-level dominate the atmospheric circulation, and strongly relate to the observed cloud bands (Fletcher et al., 2020). The structure of the flow beneath the cloud level has been investigated by several of the instruments on board the Juno spacecraft by means of gravity, infrared, and microwave measurements (Bolton et al., 2017). Particularly, the gravity measurements were used to infer that the zonal winds extend down to roughly 3,000 km, and that the main north-south asymmetry in the cloud-level wind extends to these great depths (Kaspi et al., 2018), resulting in the substantial values of the odd gravity harmonics J_3, J_5, J_7, and J_9. The excellent match between the sign and value of the predicted odd harmonics using the cloud-level wind (Kaspi, 2013) and the Juno gravity measurements (Durante et al., 2020; Iess et al., 2018), led to the inference that the wind profile at depth is similar to that at the cloud level (Kaspi et al., 2018, 2020). Here, we revisit in more detail the relation between the exact meridional profile of the zonal flow and the gravity measurements, and study how much of the cloud-level wind must be retained to match the gravity measurements.

Since the gravity measurements are sensitive to mass distribution, they are not very sensitive to the shallow levels (0.5–240 bar) probed by Juno's microwave radiometer (MWR; Janssen et al., 2017), as the density

in this region is low compared to the deeper levels. Yet, the gravity measurements have substantial implications on the MWR region, since if the flow profile at depth (below the MWR region) resembles that at the cloud level it is likely that the flow profile within the MWR region is not very different. In such a case, where the flow is barotropic, this implies via thermal wind balance that latitudinal temperature gradients in the MWR region are small, which has important implication to the MWR analysis of water and ammonia distribution (Ingersoll et al., 2017; C. Li et al., 2017, 2020). Thus, it is important to determine how strong the gravity constraint on the temperature distribution is, and what is its latitudinal dependence.

The determination of the zonal flow field at depth is based on the measurements of the odd gravity harmonics, J_3, J_5, J_7, and J_9, which are uniquely related to the flow field (Kaspi, 2013). Using only four numbers to determine a two-dimensional (latitude and depth) field poses a uniqueness challenge, and solutions that are unrelated to the observed cloud-level wind can be found (Kong et al., 2018), although the origin of such internal flow structure, completely unrelated to the cloud-level winds, is not clear. In addition, these solutions require a flow of about 1 m s^{-1} at depth of 0.8 the radius of Jupiter (~15,000 km), where the significant conductivity (Liu et al., 2008; Wicht et al., 2019) is expected to dampen such strong flows (Cao & Stevenson, 2017; Duer et al., 2019; Moore et al., 2019). Recently, Galanti & Kaspi (2021) showed that the interaction of the flow with the magnetic field in the semiconducting region can be used as an additional constraint on the structure of the flow below the cloud level. With some modification of the observed cloud-level wind (up to 10 m s^{-1}), well within its uncertainty range (Tollefson et al., 2017), a solution can be found that explains the odd gravity harmonics and abides the magnetic field constraints.

All of the abovementioned studies assumed that if the internal flow is related to the observed surface winds, it will manifest its entire latitudinal profile. However, some evidence suggests that at some latitudinal regions the flow below the clouds might be different from the winds at the cloud level. The Galileo probe, entering the Jovian atmosphere around planetocentric latitude 6.5°N (Orton et al., 1998), measured winds that strengthened from 80 ms^{-1} at the cloud level to ~160 m s^{-1} at a depth of 4 bars, from where it remains approximately constant until a depth of 20 bars where the probe stopped transmitting data (Atkinson et al., 1998). Such a baroclinic shear got further support in studies of equatorial hot spots (Choi et al., 2013; L. Li et al., 2006). Recently, Duer et al. (2020) showed that the MWR measurements of brightness temperature correlate to the zonal wind's latitudinal profile. They found that profiles differing to a limited extent from the cloud level can still be consistent with both MWR and gravity. Emanating from the correlations between MWR and the zonal winds, Fletcher et al. (2021) suggested that the winds at some latitudes might strengthen from the cloud level to a depth of 4–8 bars, that is, not far from where water is expected to be condensing, and only then begin to decay downward. Alternatively, based on stability considerations, it was suggested that while westward jets are not altered much with depth, the eastward jets might increase by 50%–100% (Dowling, 1995, 2020).

Furthermore, in the Kaspi et al. (2018) and Galanti & Kaspi (2021) studies, the observed cloud-level wind has been assumed to be projected into the planet interior along the direction parallel to the spin axis of Jupiter, based on theoretical arguments (Busse, 1970, 1976) and 3D simulations of the flow in a Jovian-like planet (e.g., Busse, 1994; Christensen, 2001; Heimpel et al., 2016; Kaspi et al., 2009). Theoretically, this requires the flow to be nearly barotropic, which is not necessarily the case, particularly when considering the three-dimensional (3D) nature of the planetary interior. Another assumption made is that the flow decays in the radial direction. This was based on the reasoning that any mechanism acting to decay the flow, such as the increasing conductivity (Cao & Stevenson, 2017), compressibility (Kaspi et al., 2009), or the existence of a stable layer (Christensen et al., 2020; Debras & Chabrier, 2019), will depend on pressure and temperature, which to first order are a function of depth. However, if the internal flow is organized in cylinders it might be the case that the mechanism acting to decay strengthens also in the direction parallel to the spin axis.

Here, we investigate what can be learned about the questions discussed above, based on the measured gravity field, considering both the symmetric and asymmetric components of the gravity field measurements. We study the ability to fit the gravity measurements with a cloud-level wind that is limited to a specific latitudinal range, thus identifying the regions where the observed cloud-level wind is likely to extend deep, and the regions where the interior flow might differ (Section 3). We also examine whether a stronger wind at the 4–8 bar level is compatible with the gravity measurements, and if the assumptions regarding the

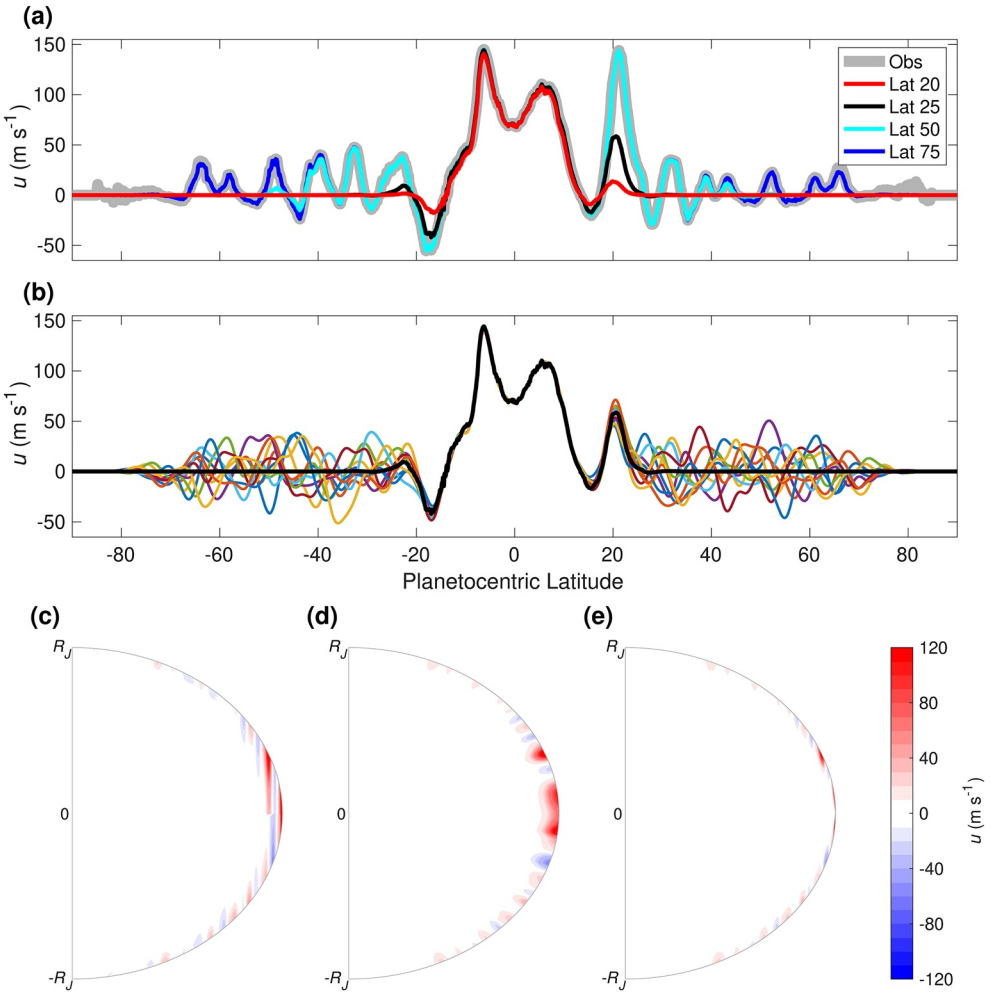

Figure 1. (a) The observed wind (Tollefson et al., 2017, gray), and variant examples with the wind truncated poleward of the latitudes 20°, 25°, 50°, and 75°. (b) The case of wind truncated poleward of the 25° latitude (black), along with examples of random winds added in the truncated regions. (c–e) Options of cloud-level wind projection and decay profiles (latitude-depth cross-section), shown as an example of a sharp decay at a 3,000-km distance from the surface. (c) Projection in the direction parallel to the spin axis and decay in the radial direction. (d) Projection and decay in the radial direction. (e) Projection and decay in the direction parallel to the spin axis.

relation of the internal flow to the cloud level can be relaxed (Section 4). Finally, we examine the latitudinal dependence of the wind-induced gravity harmonics when magnetohydrodynamics considerations are used as additional constraints (Section 5).

2. Defining the Cloud-Level Wind and Possible Internal Flow Structures

We examine several aspects of the flow structure that might influence the ability to explain the gravity measurements. First, stemming from the notion that at some latitudinal regions the flow below the cloud level might differ from the observed, we set cases in which the cloud-level wind is truncated at a specific latitude (Figure 1a). The truncation is done by applying a shifted hemispherically symmetric hyperbolic tangent function with a transition width of 5°, to allow a smooth truncation of the wind from the observed flow. The result is a wind profile that 5° equatorward of the truncation latitude is kept as in the cloud-top observations, and poleward to that latitude is practically zero (see supporting information [SI] for detailed derivation). We examine 18 cases with truncation latitudes 5°, 10°, 15°, ..., 90°. Note that all of the cloud-level wind setups used in this study are based on the analysis of the HST Jupiter images during Juno's PJ3 (Tollefson et al., 2017) (Figure 1a, gray line), and that in all figures and calculations we use the planetocentric latitude.

Next, we examine cases in which a different wind structure exists poleward of the truncation latitude. As such, unknown wind structures could replace the observed cloud-level wind at shallow depths of around 5–10 bars (e.g., as can be inferred from MWR, depending on how microwave brightness temperatures are interpreted, see Fletcher et al., 2021). For the purpose of the gravity calculation, we treat these wind profiles as if they replace the wind at the cloud level (the variation of the wind between 1 and 10 bars has a negligible effect on the induced gravity field). The observed wind is truncated poleward of 25°S–25°N, and replaced with 1,000 random wind structures that mimic the latitudinal scale and strength of the observed winds (Figure 1b, see SI for detailed methodology).

The cloud-level wind profile is first projected inward in the direction parallel to the spin axis (Kaspi et al., 2010), and then made to decay radially assuming a combination of functions (Figure 1c), that allows a search for the optimal decay profile (Kaspi et al., 2018; Galanti & Kaspi, 2021, see also SI). In addition, we examine two other cases: A case in which the cloud-level wind is both projected and decays in the radial direction (Figure 1d), and a case in which the wind is both projected and decays in the direction of the spin axis (Figure 1e).

Given a zonal flow structure, thermal wind balance is used to calculate an anomalous density structure associated with large-scale flow in fast rotating gas giants. The density field is then integrated to give the 1-bar gravity field in terms of the zonal gravity harmonics (Kaspi et al., 2010, 2016). Using an adjoint-based optimization, a solution for the flow structure is searched for, such that the model solution for the gravity field is best fitted to the part of the measured gravity field that can be attributed to the wind (Galanti & Kaspi, 2016). The odd gravity harmonics are attributed solely to the wind; therefore, we use the Juno latest measured values $J_3 = (-4.50 \pm 0.33) \times 10^{-8}$, $J_5 = (-7.23 \pm 0.42) \times 10^{-8}$, $J_7 = (12.02 \pm 1.20) \times 10^{-8}$, and $J_9 = (-11.30 \pm 3.63) \times 10^{-8}$ (Durante et al., 2020). The lowest even harmonics J_2 and J_4 are dominated by the planet's density structure and shape and cannot be used in our analysis, but interior models can give a reasonable estimate for the expected wind contribution for the higher even harmonics J_6, J_8, and J_{10} (Guillot et al., 2018). Based on the Juno measurements and the range of interior model solutions, the expected wind-induced even harmonics are estimated as $\Delta J_6 = 1 \times 10^{-8} \pm \sqrt{0.67^2 + 2^2} \times 10^{-8}$, $\Delta J_8 = 3.5 \times 10^{-8} \pm \sqrt{2.1^2 + 0.5^2} \times 10^{-8}$, and $\Delta J_{10} = -3 \times 10^{-8} \pm \sqrt{6.5^2 + 0.25^2} \times 10^{-8}$. The two uncertainties associated with each even harmonic are from two independent sources, the measurement uncertainty and the uncertainty due to internal models (respectively), so that the overall uncertainty is calculated as their root sum of squares.

Finally, to isolate the latitudinal dependence of the wind-induced gravity signal from the general ability to fit the gravity harmonics, we first optimize the cloud-level wind so that the odd gravity harmonics are fitted perfectly (Galanti & Kaspi, 2021). The modified wind is very similar to the observed (Figure S1), well within the uncertainty of the cloud-level wind observation (Tollefson et al., 2017), therefore retaining all the observed latitudinal structure responsible for the wind-induced gravity harmonics.

3. The Latitudinal Sensitivity of the Wind-Induced Gravity Field

We begin by analyzing the effect of the cloud-level wind latitudinal truncation on the ability to explain the gravity harmonics. For each wind setup, the internal flow structure is modified until the best fit to the four odd harmonics and the three even harmonics are reached (Figure 2). The cost function (Figure 2a), a measure for the overall difference between the measurements and the model solution (see SI), reveals the contribution of each latitudinal region to the solution. First, as expected, when the cloud-level wind is retained at all latitudes, the solution for the odd harmonics is very close to the measurements (Figures 2b–2d, red dots). Importantly, the same optimal flow structure explains very well the even harmonics (Figures 2e and 2f, red dots). This is additional evidence that the observed cloud-level wind is dynamically related to the gravity field.

Examining the latitudinal dependence of the truncation, it is evident that truncating the observed cloud-level wind closer to the equator than 25°S–25°N prevents any flow structure that could explain the gravity harmonics. It is most apparent in the odd harmonics (Figures 2b–2d) where the optimal solutions (dark blue circles) are close to zero and far from the measured values. It is also the case for ΔJ_8, but for ΔJ_6 and ΔJ_{10} the solutions are inside the uncertainty: In ΔJ_6 because the measured value is very small, and in ΔJ_{10} because the uncertainty is very large. Considering the cloud-level wind profile (Figure 1a, black), it is not surprising

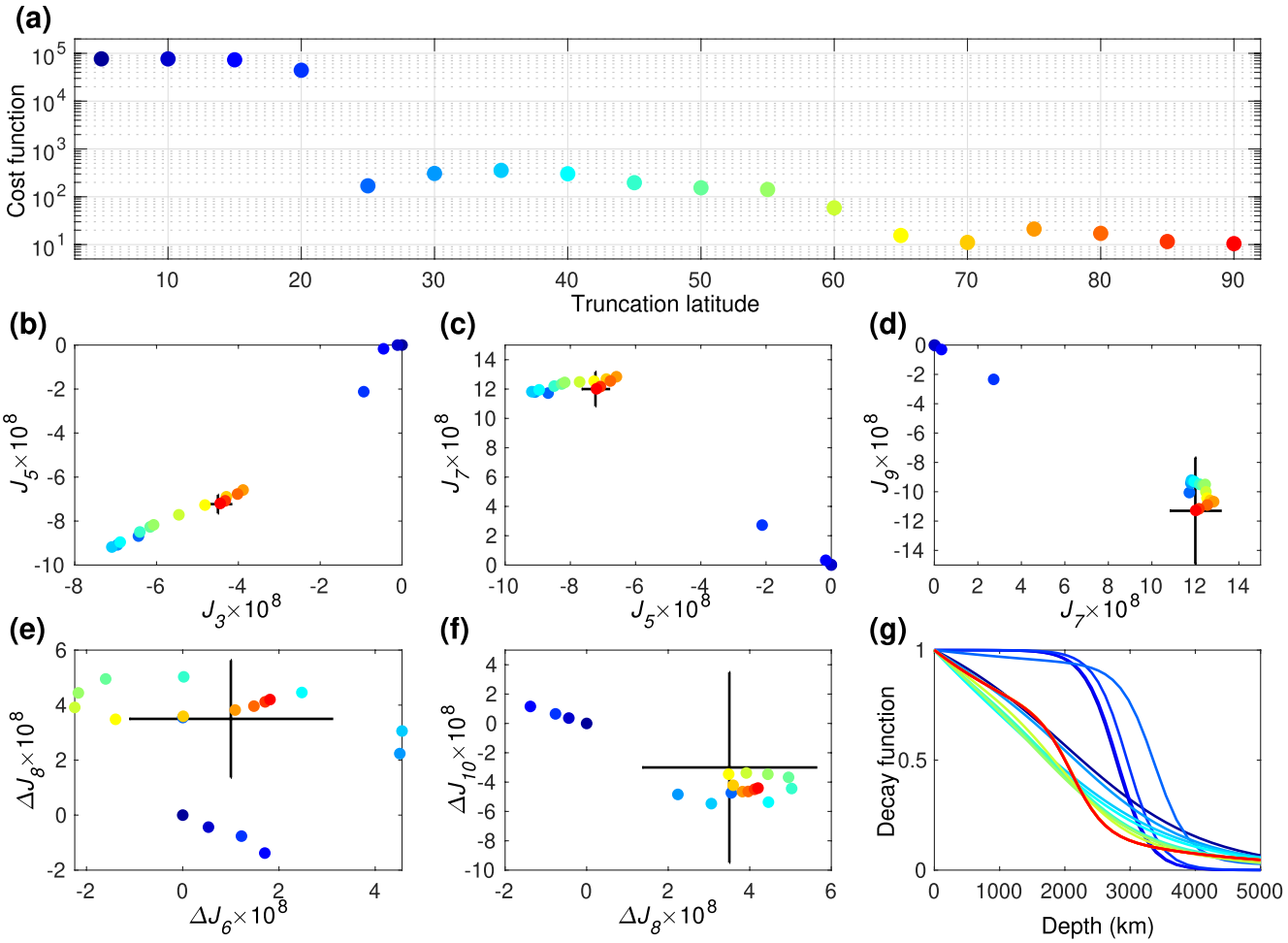

Figure 2. Latitude-dependent solutions as function of the truncation latitude. (a) The overall fit of the model solution to the measurements (cost function). Each case is assigned with a different color that is used in the following panels, ranging from latitude 5° (blue) to 90° (no truncation, red). (b–f) The solutions for the different gravity harmonics (colors) and the measurement (black). (g) The decay function associated with each solution.

that truncating the winds poleward of 25°S–25°N makes the difference in the solution, as this is where the asymmetric positive (negative) jet in the northern (southern) hemisphere is found, and projects strongly on the low order odd harmonics. Note that even a 5° difference (Figure 1a, red, truncation at 20°S–20°N) prevents a physical solution from being reached. Once these opposing jets are included, the flow structure contains enough asymmetry to explain very well J_7 and J_9, which have the largest values of the odd harmonics.

However, with the 25°S–25°N truncation, the model solutions for J_3 and J_5 are still outside the measured uncertainty. Only when the influence of the zonal winds throughout the 60°S–60°N range (Figure 1a, yellow) is included, then the lower odd harmonics can be explained with the cloud-level wind profile. The optimal decay function for each case (Figure 2g), emphasizes the robustness of the solutions. When only the equatorial region is retained, the optimization is trying (with no success) to include as much mass in the region where the cloud-level wind is projected inward. Even when the wind is truncated at 20°, the deepest wind (located at the equatorial plane) is at $H = R_J\left[1 - \cos(20\pi / 180)\right] \sim 4{,}000$ km, so that solutions deeper than 4,000 km do not add mass to the gravity solution. But once the winds at 25°S–25°N are included, then the decay function of the wind settles on a similar profile, with some small variations between the cases (Figure 2g). Note that repeating these experiments with the exact Tollefson et al. (2017) cloud-level wind profile, does not change substantially the main results (Figure S2), thus ensuring their robustness.

The same methodology can be applied to a cloud-level wind that is truncated equatorward of a latitudinal region (Figure S3). The analysis shows that a wind truncated equatorward of a latitude larger than

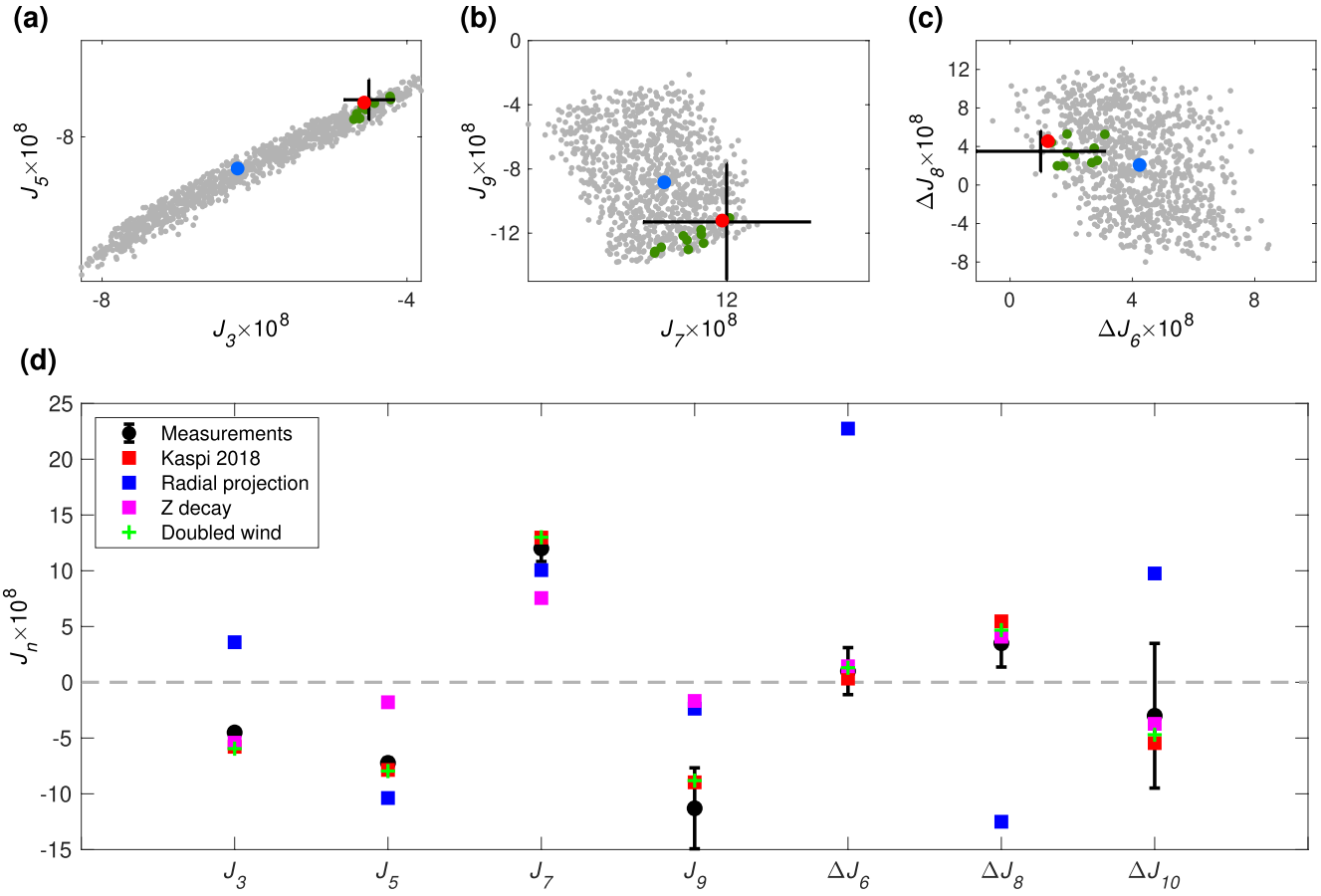

Figure 3. (a–c) Solutions with the cloud-level wind truncated poleward of 25°S–25°N and replaced with random jets there (Figure 1b). Shown are the solutions for 1,000 random cases (gray), and within those the solution which matches all the gravity harmonics (green). Also shown are the solution with no random winds (blue, corresponding to the 25° case in Figure 2), the solution with no truncation of the winds (red, corresponding to the 90° case in Figure 2), and the Juno measurements (black). (d) Solutions for cases with cloud-level wind projected in the radial direction (blue; Figure 1d), wind decayed in the direction parallel to the spin axis (magenta; Figure 1e), and a doubled cloud-level wind (green). Also shown are the measurements (black), and the solution with the unaltered cloud-level wind (red; Kaspi et al., 2018).

25°S–25°N does not allow a plausible solution to be reached. Consistently with the above experiment, the deep jets at 25°S–25°N are necessary to fit gravity harmonics. Specifically, there is a gradual deterioration of the solution in the truncation region of 0°–20°, which is related solely to the even harmonics ΔJ_6, ΔJ_8, and ΔJ_{10}. Once the wind is truncated inside 10°S–10°N the solution for ΔJ_6 and ΔJ_8 is outside the uncertainty range, and ΔJ_{10} moves further away from the measurement. This is due to the strong eastward jets at 6°S and 6°N.

4. Variants of the Flow Structure

Next, we examine several variants of the wind setups. In Section 3, we showed that the jets between 25°S and 25°N are crucial for explaining the gravity harmonics, and therefore should not differ much below the cloud level. However, in the regions poleward to the truncation latitude it should be examined whether a flow below the cloud level, which is completely different, might still allow matching the gravity harmonics. We therefore examine a case where the cloud-level wind is truncated poleward of 25°S–25°N, and in the truncated regions random jets are added to simulate different possible scenarios (Figure 1b, see SI for definition). The gravity harmonic solutions for 1,000 different cases are shown in Figures 3a–3c. The largest effect the random jets have is on J_3 and J_5, with considerable effect also on the other odds and even harmonics. About 1% of the cases provide a good match to all the measurements (green), therefore it is still statistically possible (although not likely) that some combination of jets unseen at the cloud level at the midlatitudes,

with amplitude of up to ± 40 m s^{-1}, are responsible for part of the gravity signal. These results are consistent with Duer et al. (2020) who did a similar analysis, but taking the full cloud-level winds and showed that solutions differing from the cloud level are possible but statistically unlikely (~1%). Doubling (halving) the random jets' strength results in only 0.2% (0%) of the solutions to fit the gravity measurement (Figure S7), suggesting that if alternative jets exist in the midlatitudes, their amplitude should be around ±40 m s^{-1}.

Aside from modifications to the cloud-level wind, we also examine cases in which the projection of the flow beneath the cloud level is modified. For simplicity, we examine these cases with the observed cloud-level wind spanning the full latitudinal range. Projecting the wind radially and keeping the decay radial (Figure 1d), we find that there is no plausible solution for flow structure under these assumptions that would give a good fit to the gravity measurements (Figure 3d, blue). The best-fit model solution for all J_n is far from the measurements, well outside their uncertainty range, and does not even match J_3 and J_8 in sign. Next, we consider a case in which the decay of the winds is in the direction parallel to the spin axis (Figure 1e). Here the optimal solution for the odd harmonics J_5, J_7, and J_9 is far from the measured values (Figure 3d, magenta), while for J_3 and the even harmonics the solution is within the uncertainty range. However, in this case, the winds needs to be very deep, extending to ~5,000 km, where the interaction with the magnetic field is extremely strong (Cao & Stevenson, 2017; Galanti & Kaspi, 2021; Galanti et al., 2017). Finally, following the suggestion that the cloud-level wind might get stronger with depth before they decay (e.g., Fletcher et al., 2021), we conduct an experiment in which we double the cloud-level wind. Interestingly, a plausible solution can be achieved (Figure 3d, green crosses), with a decay profile similar to the Kaspi et al. (2018) solution, but with the winds decaying more baroclinicity in the upper 2,000 km, and then decaying slower (Figure S6).

5. Adding Magnetohydrodynamic Constraints

In Jupiter, the increased conductivity with depth (e.g., French et al., 2012; Wicht et al., 2019) suggests that the flow might be reduced to very small values in the semiconducting region (deeper than 2,000 km, Cao & Stevenson, 2017). Using flow estimates in the semiconducting region based on past magnetic secular variations (Moore et al., 2019), Galanti & Kaspi (2021) gave a revised wind decay profile that can explain both the gravity harmonics and the constraints posed by the secular variations. We follow this approach, setting the flow strength in the semiconducting region (deeper than 2,000 km, see Galanti & Kaspi, 2021) to be a sharp exponential function (Figure 4g, right part). Given this inner profile of the decay function, the outer part of the decay function can be searched for, together with the optimal latitudinal wind profile, that will result in the best fit to the odd measured gravity harmonics. The optimal wind profile (Figure S1b) is very similar to the observed wind, with deviations that are within the uncertainties.

Using the modified cloud-level wind, the shape of the decay function in the outer neutral region is optimized to allow the best-fit to the odd and even gravity harmonics (Figures 4b–4g). In addition to the odd harmonics, which are expected to fit the measurements, the model also fits very well the even harmonics, despite the limited range of possible decay profiles in the outer region (Figure 4g). The latitudinal dependence reveals that the range of 60°S–60°N is needed to allow a good fit, especially for J_3 and J_7. Similar to the case with gravity-only constraints, fitting the even harmonics, as well as J_5 and J_9, requires mostly the cloud-level wind inside the 25°S–25°N region. Thus, even when including the strong magnetic constraint, the dominance of the 25°S–25°N region remains robust.

6. Conclusion

Given the Juno gravity measurements, which latitudinal range of Jupiter's observed cloud-level wind is extending down deep into the planet? This is the question we set to answer in this study, defining the wind-related gravity field not only with the odd harmonics, as was done in previous studies (Kaspi et al., 2018), but also with the higher even harmonics residuals ΔJ_6, ΔJ_8, and ΔJ_{10} (Guillot et al., 2018; Kaspi et al., 2020). We show that the latitudinal range of 25°S–25°N holds most of the wind signal needed to explain the measured gravity field. The winds at the midlatitudes contribute as well to the gravity field, mostly to the odd harmonics, and to match fully the measured gravity signal the winds in the latitudinal range 60°S–60°N must extend deep. Specifically, the odd harmonics have a large contribution from the opposing jets at 20°S and

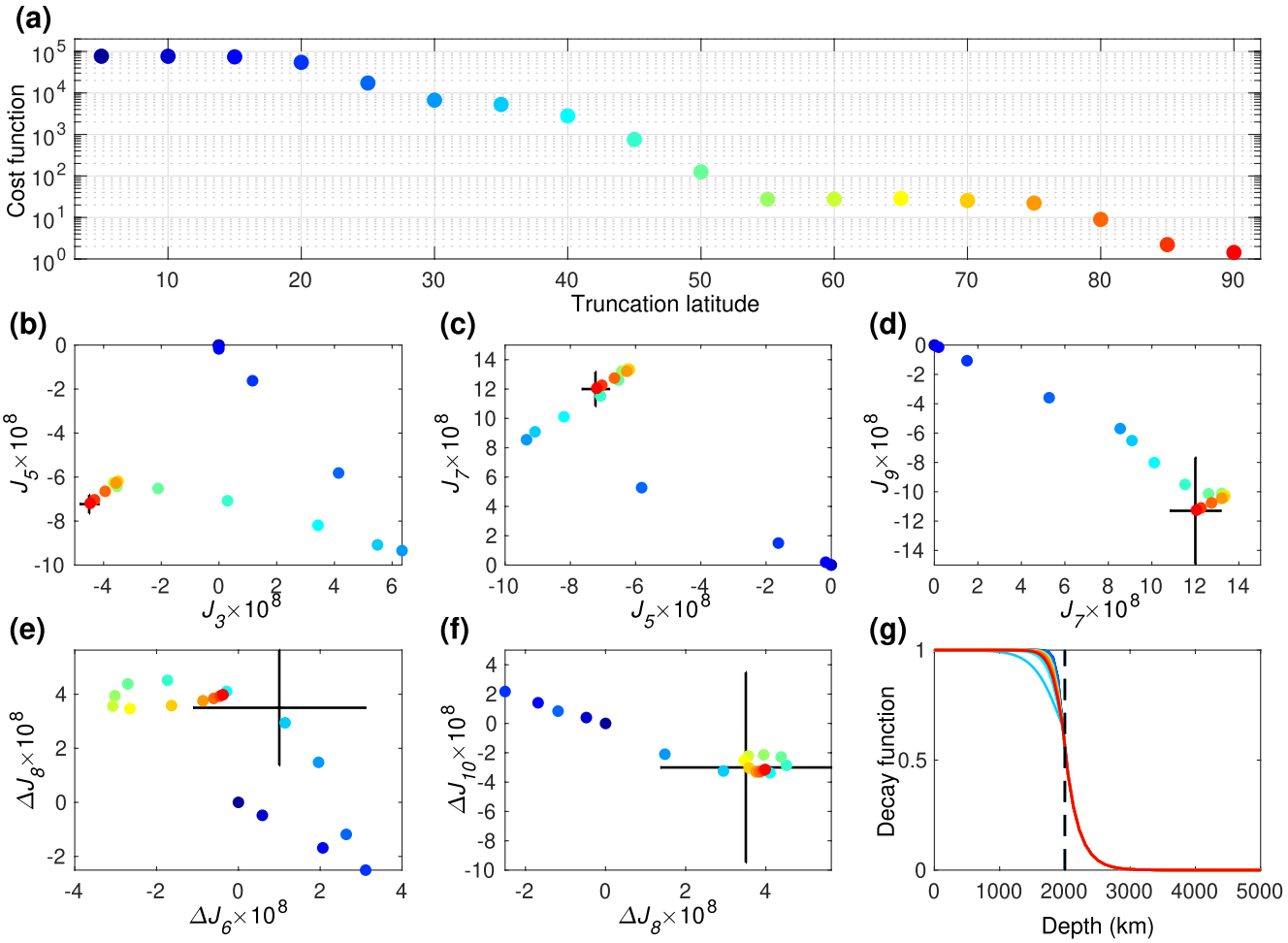

Figure 4. Same as Figure 2, but for a case where the flow profile in the semiconducting region is restricted to comply with secular variations consideration (Duer et al., 2019; Moore et al., 2019). The black dashed line in panel (g) denotes the separation between the outer-neutral and inner-semiconducting regions.

20°N, while the even harmonics are dominated by the eastward jets at 6°S and 6°N. Adding random jets poleward of 25°S–25°N enlarges the range of solutions, and for specific setups of the random jets, a good match to the gravity harmonics can be found, implying that midlatitude jet structures might somewhat differ from those observed at the cloud-tops.

We also find that projecting the winds inward in the radial direction does not allow any plausible solutions to be found, and so is the case for flows that are decayed in the direction parallel to the spin axis of Jupiter. These experiments strengthen the validity of the two physical assumptions taken in relating the internal flow structure to the cloud-level winds. First, that the interior flow is organized in cylinders reflecting the cloud-level winds, and second, that the flow decays in the radial direction due to processes depending on pressure and temperature.

In addition to the measurements of the seven, odd and even, gravity harmonics, we also consider a case where constraints on the flow in the semiconducting region, arising from consideration of magnetic secular variations (Moore et al., 2019), are imposed. We find that, with small alterations of the cloud-level winds, a flow structure can be found such that all gravity harmonics are explained, and that in general the latitudinal dependence of the solutions is similar to that found with gravity-only constraints.

Data Availability Statement

Data are available through Iess et al. (2018), Guillot et al. (2018), and Galanti & Kaspi (2021).

Acknowledgments
E. Galanti, Y. Kaspi and K. Duer are supported by the Israeli Space Agency and the Helen Kimmel Center for Planetary Science at the Weizmann Institute of Science. L. Fletcher is a Juno Participating Scientist supported by a Royal Society Research Fellowship and European Research Council Consolidator Grant (under the European Union's Horizon 2020 research and innovation programme, grant agreement No 723890) at the University of Leicester. Some of this research was carried out at the Jet Propulsion Laboratory, California Institute of Technology, under a contract with the National Aeronautics and Space Administration (80NM0018D0004). All authors have been supported by the Juno project.

References

Atkinson, D. H., Pollack, J. B., & Seiff, A. (1998). The Galileo probe doppler wind experiment: Measurement of the deep zonal winds on Jupiter. *Journal of Geophysical Research*, *103*, 22911–22928. https://doi.org/10.1029/98JE00060

Bolton, S. J., Adriani, A., Adumitroaie, V., Allison, M., Anderson, J., Atreya, S., et al. (2017). Jupiter's interior and deep atmosphere: The initial pole-to-pole passes with the Juno spacecraft. *Science*, *356*, 821–825. https://doi.org/10.1126/science.aal2108

Busse, F. H. (1970). Thermal instabilities in rapidly rotating systems. *Journal of Fluid Mechanics*, *44*, 441–460. https://doi.org/10.1017/S0022112070001921

Busse, F. H. (1976). A simple model of convection in the Jovian atmosphere. *Icarus*, *29*, 255–260. https://doi.org/10.1016/0019-1035(76)90053-1

Busse, F. H. (1994). Convection driven zonal flows and vortices in the major planets. *Chaos*, *4*(2), 123–134. https://doi.org/10.1063/1.165999

Cao, H., & Stevenson, D. J. (2017). Zonal flow magnetic field interaction in the semi-conducting region of giant planets. *Icarus*, *296*, 59–72. https://doi.org/10.1016/j.icarus.2017.05.015

Choi, D. S., Showman, A. P., Vasavada, A. R., & Simon-Miller, A. A. (2013). Meteorology of Jupiter's equatorial hot spots and plumes from Cassini. *Icarus*, *223*(2), 832–843. https://doi.org/10.1016/j.icarus.2013.02.001

Christensen, U. R. (2001). Zonal flow driven by deep convection in the major planets. *Geophysical Research Letters*, *28*, 2553–2556. https://doi.org/10.1029/2000GL012643

Christensen, U. R., Wicht, J., & Dietrich, W. (2020). Mechanisms for limiting the depth of zonal winds in the gas giant planets. *Acta Pathologica Japonica*, *890*(1), 61. https://doi.org/10.3847/1538-4357/ab698c

Debras, F., & Chabrier, G. (2019). New models of Jupiter in the context of Juno and Galileo. *Acta Pathologica Japonica*, *872*, 100. https://doi.org/10.3847/1538-4357/aaff65

Dowling, T. E. (1995). Estimate of Jupiter's deep zonal-wind profile from shoemaker-levy 9 data and Arnol'd's second stability criterion. *Icarus*, *117*, 439–442. https://doi.org/10.1006/icar.1995.1169

Dowling, T. E. (2020). Jupiter-style jet stability. *Planetary Science Journal*, *1*, 6. https://doi.org/10.3847/PSJ/ab789d

Duer, K., Galanti, E., & Kaspi, Y. (2019). Analysis of Jupiter's deep jets combining Juno gravity and time-varying magnetic field measurements. *Acta Pathologica Japonica*, *879*(2), L22. https://doi.org/10.3847/2041-8213/ab288e

Duer, K., Galanti, E., & Kaspi, Y. (2020). The range of Jupiter's flow structures that fit the Juno asymmetric gravity measurements. *Journal of Geophysical Research: Planets*, *125*(8), e06292. https://doi.org/10.1029/2019JE006292

Durante, D., Parisi, M., Serra, D., Zannoni, M., Notaro, V., Racioppa, P., et al. (2020). Jupiter's gravity field halfway through the Juno mission. *Geophysical Research Letters*, *47*(4), e86572. https://doi.org/10.1029/2019GL086572

Fletcher, L. N., Kaspi, Y., Guillot, T., & Showman, A. P. (2020). How well do we understand the belt/zone circulation of giant planet atmospheres? *Space Science Reviews*, *216*(2), 30. https://doi.org/10.1007/s11214-019-0631-9

Fletcher, L. N., Oyafuso, F. A., Allison, M. D., Ingersoll, A., Li, L., Kaspi, Y., et al. (2021). Jupiter's temperate belt/zone contrasts revealed at depth by Juno microwave observations. *Earth and Space Science Open Archive*, 35. https://doi.org/10.1002/essoar.10506297.1

French, M., Becker, A., Lorenzen, W., Nettelmann, N., Bethkenhagen, M., Wicht, J., & Redmer, R. (2012). Ab initio simulations for material properties along the Jupiter adiabat. *Astrophysical Journal Supplement*, *202*(1), 5. https://doi.org/10.1088/0067-0049/202/1/5

Galanti, E., Cao, H., & Kaspi, Y. (2017). Constraining Jupiter's internal flows using Juno magnetic and gravity measurements. *Geophysical Research Letters*, *44*(16), 8173–8181. https://doi.org/10.1002/2017GL074903

Galanti, E., & Kaspi, Y. (2016). An adjoint-based method for the inversion of the Juno and Cassini gravity measurements into wind fields. *Acta Pathologica Japonica*, *820*(2), 91. https://doi.org/10.3847/0004-637X/820/2/91

Galanti, E., & Kaspi, Y. (2021). Combined magnetic and gravity measurements probe the deep zonal flows of the gas giants. *Monthly Notices of the Royal Astronomical Society*, *501*(2), 2352–2362. https://doi.org/10.1093/mnras/staa3722

Galanti, E., Kaspi, Y., & Tziperman, E. (2017). A full, self-consistent treatment of thermal wind balance on oblate fluid planets. *Journal of Fluid Mechanics*, *810*, 175–195. https://doi.org/10.1017/jfm.2016.687

Guillot, A. P., Adumitroaie, V., Allison, M. D., Atreya, S., Bellotti, A. A., Bolton, S. J., et al. (2017). Implications of the ammonia distribution on Jupiter from 1 to 100 bars as measured by the Juno microwave radiometer. *Geophysical Research Letters*, *44*(15), 7676–7685. https://doi.org/10.1002/2017GL074277

Guillot, T., Miguel, Y., Militzer, B., Hubbard, W. B., Kaspi, Y., Galanti, E., et al. (2018). A suppression of differential rotation in Jupiter's deep interior. *Nature*, *555*, 227–230. https://doi.org/10.1038/nature25775

Heimpel, M. H., Gastine, T., & Wicht, J. (2016). Simulation of deep-seated zonal jets and shallow vortices in gas giant atmospheres. *Nature Geoscience*, *9*, 19–23. https://doi.org/10.1038/ngeo2601

Iess, L., Folkner, W. M., Durante, D., Parisi, M., Kaspi, Y., Galanti, E., et al. (2018). Measurement of Jupiter's asymmetric gravity field. *Nature*, *555*, 220–222. https://doi.org/10.1038/nature25776

Janssen, M. A., Oswald, J. E., Brown, S. T., Gulkis, S., Levin, S. M., Bolton, S. J., et al. (2017). MWR: Microwave radiometer for the Juno mission to Jupiter. *Space Science Reviews*, *213*(1–4), 139–185. https://doi.org/10.1007/s11214-017-0349-5

Kaspi, Y. (2013). Inferring the depth of the zonal jets on Jupiter and Saturn from odd gravity harmonics. *Geophysical Research Letters*, *40*, 676–680. https://doi.org/10.1029/2012GL053873

Kaspi, Y., Davighi, J. E., Galanti, E., & Hubbard, W. B. (2016). The gravitational signature of internal flows in giant planets: Comparing the thermal wind approach with barotropic potential-surface methods. *Icarus*, *276*, 170–181. https://doi.org/10.1016/j.icarus.2016.04.001

Kaspi, Y., Flierl, G. R., & Showman, A. P. (2009). The deep wind structure of the giant planets: Results from an anelastic general circulation model. *Icarus*, *202*(2), 525–542. https://doi.org/10.1016/j.icarus.2009.03.026

Kaspi, Y., Galanti, E., Hubbard, W. B., Stevenson, D. J., Bolton, S. J., Iess, L., et al. (2018). Jupiter's atmospheric jet streams extend thousands of kilometres deep. *Nature*, *555*, 223–226. https://doi.org/10.1038/nature25793

Kaspi, Y., Galanti, E., Showman, A. P., Stevenson, D. J., Guillot, T., Iess, L., & Bolton, S. J. (2020). Comparison of the deep atmospheric dynamics of Jupiter and Saturn in light of the Juno and Cassini gravity measurements. *Space Science Reviews*, *216*(5), 84. https://doi.org/10.1007/s11214-020-00705-7

Kaspi, Y., Hubbard, W. B., Showman, A. P., & Flierl, G. R. (2010). Gravitational signature of Jupiter's internal dynamics. *Geophysical Research Letters*, *37*. https://doi.org/10.1029/2009GL041385

Kong, D., Zhang, K., Schubert, G., & Anderson, J. D. (2018). Origin of Jupiter's cloud-level zonal winds remains a puzzle even after Juno. *Proceedings of the National Academy of Sciences of the United States of America*, *115*(34), 8499–8504. https://doi.org/10.1073/pnas.1805927115

Li, C., Ingersoll, A., Bolton, S., Levin, S., Janssen, M., Atreya, S., et al. (2020). The water abundance in Jupiter's equatorial zone. *Nature Astronomy*, *4*, 609–616. https://doi.org/10.1038/s41550-020-1009-3

Li, C., Ingersoll, A., Janssen, M., Levin, S., Bolton, S., Adumitroaie, V., et al. (2017). The distribution of ammonia on Jupiter from a preliminary inversion of Juno microwave radiometer data. *Geophysical Research Letters*, *44*(11), 5317–5325. https://doi.org/10.1002/2017GL073159

Li, L., Ingersoll, A. P., Vasavada, A. R., Simon-Miller, A. A., Del Genio, A. D., Ewald, S. P., et al. (2006). Vertical wind shear on Jupiter from Cassini images. *Journal of Geophysical Research*, *111*(E4), E04004. https://doi.org/10.1029/2005JE002556

Liu, J., Goldreich, P., & Stevenson, D. (2008). Constraints on deep-seated zonal winds inside Jupiter and Saturn. *Icarus*, *196*, 653–664. https://doi.org/10.1016/j.icarus.2007.11.036

Moore, K. M., Cao, H., Bloxham, J., Stevenson, D. J., Connerney, J. E. P., & Bolton, S. J. (2019). Time variation of Jupiter's internal magnetic field consistent with zonal wind advection. *Nature Astronomy*, *3*, 730–735. https://doi.org/10.1038/s41550-019-0772-5

Orton, G. S., Fisher, B. M., Baines, K. H., Stewart, S. T., Friedson, A. J., Ortiz, J. L., et al. (1998). Characteristics of the Galileo probe entry site from Earth-based remote sensing observations. *Journal of Geophysical Research*, *103*, 22791–22814. https://doi.org/10.1029/98JE02380

Tollefson, J., Wong, M. H., de Pater, I., Simon, A. A., Orton, G. S., Rogers, J. H., et al. (2017). Changes in Jupiter's zonal wind profile preceding and during the Juno mission. *Icarus*, *296*, 163–178. https://doi.org/10.1016/j.icarus.2017.06.007

Wicht, J., Gastine, T., Duarte, L. D. V., & Dietrich, W. (2019). Dynamo action of the zonal winds in Jupiter. *Astronomy & Astrophysics*, *629*, A125. https://doi.org/10.1051/0004-6361/201935682

References From the Supporting Information

Liu, J., Schneider, T., & Kaspi, Y. (2013). Predictions of thermal and gravitational signals of Jupiter's deep zonal winds. *Icarus*, *224*, 114–125. https://doi.org/10.1016/j.icarus.2013.01.025

Pedlosky, J. (1987). *Geophysical fluid dynamics* (p. 710). Springer-Verlag.

Zhang, K., Kong, D., & Schubert, G. (2015). Thermal-gravitational wind equation for the wind-induced gravitational signature of giant gaseous planets: Mathematical derivation, numerical method, and illustrative solutions. *Acta Pathologica Japonica*, *806*(2), 270. https://doi.org/10.1088/0004-637X/806/2/270